TÜBİTAK

Turkish Journal of Chemistry

http://journals.tubitak.gov.tr/chem/

Research Article

Turk J Chem
(2019) 43: 1183 – 1203

doi:10.3906/kim-1903-76

On the azo dyes derived from benzoic and cinnamic acids used as photosensitizers in dye-sensitized solar cells

Luka MATOVIĆ[1], Nikola TASIĆ[2], Nemanja TRIŠOVIĆ[1], Jelena LAĐAREVIĆ[1], Vesna VITNIK[3], Željko VITNIK[3], Branimir GRGUR[1], Dušan MIJIN[1,*]

[1]Faculty of Technology and Metallurgy, University of Belgrade, Belgrade, Serbia
[2]Institute for Multidisciplinary Research, University of Belgrade, Belgrade, Serbia
[3]Department of Chemistry, Institute of Chemistry, Technology and Metallurgy, University of Belgrade, Belgrade, Serbia

Received: 28.03.2019 • **Accepted/Published Online:** 14.06.2019 • **Final Version:** 06.08.2019

Abstract: In order to get a better insight into the relationship between molecular structure and photovoltaic performance, six monoazo dye molecules containing benzoic and cinnamic acid moieties were synthesized and their photovoltaic properties were studied. Three of them have not been previously used in solar cells. Spectroscopic measurements of the investigated compounds coupled with theoretical calculations were performed. Short-circuit current density, open-circuit voltage, and fill-factor were determined. It was found that a larger amount of short-circuit current density will be generated if the HOMO–LUMO energy gap is lower, determined by the stability of the molecule and the electronic effect of the donor moiety. Among both series of synthesized dye molecules, the highest obtained values of short-circuit current density were achieved with (2-hydroxynaphthalene-1-ylazo)benzoic acid and (2-hydroxynaphthalene-1-ylazo)cinnamic acid, and thus they were regarded as promising candidates for application in dye-sensitized solar cells.

Key words: Dye-sensitized solar cells, azo dyes, short-circuit current, quantum chemical calculation, solvatochromism, tautomerism

1. Introduction

The application of dye-sensitized solar cells (DSSCs), which contain a thin photoactive organic dye film deposited on a nanoporous titanium dioxide (TiO_2) layer, emerged as a brand new solid energy conversion, low-cost fabrication, and low-environmental pollution potential solar technology almost three decades ago [1–4]. The architecture of these cells represents a multicomponent system in which all factors of the device work synergistically to transform sunlight into electricity. The photosensitizer, as one of the main components, has a multifunctional role in the overall operative system of DSSCs. The absorption of incident light is very pertinent for optimum solar cell performance. In that manner, a dye molecule should be thermo- and photostable and able to absorb incident light in as wide of a UV-Vis light spectrum range as possible. For effective electron injection from the LUMO of the dye molecule to the conductive band of TiO_2, the deposition of the dye molecule should be optimal. It means that a molecule should be well adsorbed onto the metal oxide surface via an anchoring group (–COOH, $–SO_3H$, $–H_2PO_3$). In this regard, azo dyes have attracted great attention in recent years, possessing advantages over the rest of the organic photosensitive molecules. These include: (1) facile manipulation, i.e. substitution on the azo (–N=N–) chromophore, (2) high values of molar extinction

*Correspondence: kavur@tmf.bg.ac.rs

coefficients, and (3) they are cheaper to synthesize and less harmful to the environment than metal complexes. These dyes have been widely used in many fields of technology, including photoactive materials, especially DSSCs, as main competitors to both silicon solar cells and complexes based on ruthenium. Even though these molecules do not give as satisfactory a degree of incident photon-to-current conversion as inorganic molecules, azo dye solar technology is constantly progressing [1–5]. The application of azo dyes as sensitizers in DSSCs has been extensively studied from both the experimental and theoretical points of view [1,4–8].

In the present study, a complex synthetic route was developed in order to enable the parallel synthesis of a larger series of compounds. Three monoazo dye molecules were derived from benzoic acid and their three homologous derivates were obtained from cinnamic acid (Figure 1) bearing the same electron-donor moiety. The photovoltaic performance of these compounds has been measured and analyzed. Namely, compounds **2a** and **5a** have been already used in DSSCs based on nanocrystalline TiO_2 films by Nakajima et al. [1] and Prajongtat et al. [5] as well as compound **2c** by Zhang and Cole [8], and they have been chosen for comparison. Three other dyes were not used in DSSCs before.

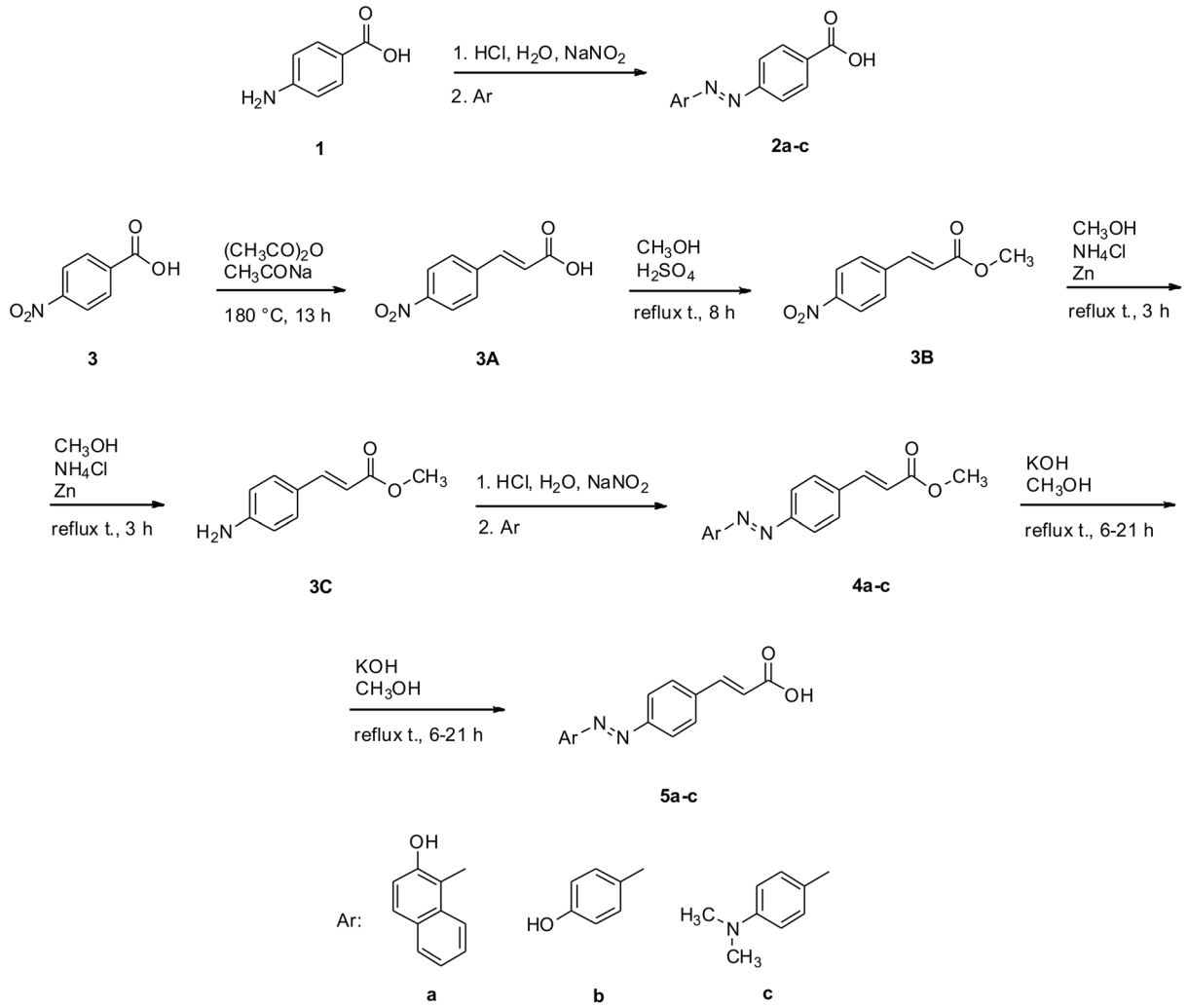

Figure 1. Reaction pathway for obtaining azo dyes derived from: benzoic acid (2) and cinnamic acid (5).

The effects of the electron-donating capability of three commonly used units in the DSSC molecule framework, namely hydroxynaphthyl, hydroxyphenyl, and N,N-dimethylphenyl, on photovoltaic performance were compared for the first time. A detailed analysis of the azo-hydrazone tautomerism enabled the identification of structural and electronic features relevant for the application of DSSCs. The presented investigation of the photosensitizer performance of the synthesized compounds, coupled with a detailed quantum chemical study, affords guidelines for the preparation of new and more effective azo dye candidates for DSSCs.

2. Experimental section

2.1. Materials and methods

All reagents and solvents used for obtaining the targeted compounds were purchased from companies such as Macron, Acros, and Aldrich and were used without further purification. The melting points of all compounds synthesized in the present study were obtained using an Electrothermal melting point apparatus. The UV absorption spectra of the dye molecules were recorded on a UV-VIS 1700 Shimadzu spectrophotometer at room temperature. All dyes were dissolved in spectral grade solvents, whereby the optical properties of the dyes were monitored within the wavelength range of 220–650 nm. The concentration of all dye solutions was uniform (5 $\times$ 10^{-5} M). FT-IR spectra were recorded using a BOMEM MB-Series spectrophotometer, within the spectral resolution range of 400–4000 cm^{-1} using KBr pellets. NMR characterization was performed on a Bruker Ascend 400 apparatus in pure DMSO, whereby ^{1}H NMR and ^{13}C NMR spectral data were gained at 400 and 100 MHz, respectively, using tetramethylsilane (TMS) as an internal standard.

2.2. The preparation of electrodes and DSSC performance testing

The DSSC assembly was made by modified procedures [8,9]. FTO glass substrates (MTI Co.) with a deposited TiO_2 (Ti-Nanoxide D/SP, Solaronix) nanoporous layer were initially washed with detergent and water and then rinsed with ethanol. A monolayer of TiO_2/Pt paste (14 μm) was applied on a well-dried FTO glass in perpendicular shape of area 0.25 cm^2 by doctor blade technique. Sintering of TiO_2 and firing platinum (Platisol T/SP, Solarnonix) layer was performed by gradually heating coated glass substrates on a hot plate to 480–485 °C. After the glass substrates with the deposited TiO_2 layer were cooled to $\sim$50 °C, the dyeing of photoelectrodes was performed by immersing the TiO_2-coated glass into the specified 0.5 mM solution of the dyes and left as such for 24 h. The azo dyes were previously dissolved in 96% ethanol and the dye solution was sonicated, boiled, and, after cooling to the room temperature, centrifuged. After the time spent in solution, the glass substrates were slightly rinsed with ethanol, dried, and 2–3 drops of electrolyte (Iodolyte Z-150, Solaronix) were applied to the TiO_2 site before DSSC assembly.

After the DSSC unit had been assembled, it was subjected to illumination (Osram halogen lamp, 120 V/300 W, 100 mW/cm^2) in order to record J_{SC}–V_{OC} curves (displayed in Section 3) and to determine the basic operating parameters of the solar cell, such as J_{SC}, V_{OC}, fill factor (ff), and solar-cell efficiency (η), consequently.

2.3. Quantum chemical investigation—a DFT analysis

To comprehend the relationship between electronic structure on the physicochemical properties of the targeted dyes, DFT analysis was performed. All calculations were carried out with the program Gaussian 09 [10].

The structures of dye molecules were optimized using the B3LYP functional [11] and M06-2X [12] with 6-311++G(d,p) basis set. The M06-2X [12] functional was chosen to simulate the absorption spectra of dyes and CT indexes. The absorption spectra of the dyes were simulated using TD-DFT and the solvent effect (ethanol) was undertaken using the conductor-like polarizable continuum model (CPCM) [13].

2.4. Synthesis of dye molecules

All azo dyes were obtained by following the synthetic routes presented in Figure 1. Dye molecules derived from benzoic acid were prepared by modified procedures [14,15]. Azo dyes with the cinnamic acid moiety were prepared by a five-step synthetic route. 4-Nitrocinnamic acid (**3A**) was prepared from 4-nitrobenzaldehyde (**3**) according to a literature procedure [16]. This acid was then esterified to obtain the methyl ester of 4-nitrocinnamic acid (**3B**) [17] followed by reduction to produce methyl 4-aminocinnamate (**3C**) [18]. The targeted azo dyes (**5a**–**c**) were synthesized via a diazotation reaction of the given amino ester followed by a coupling reaction of the resulting diazonium salt with the corresponding coupling reagents, which was subsequently hydrolyzed [19].

2.4.1. Synthesis of 4-(4-substitutedphenylazo)benzoic acids

2.4.1.1. Synthesis of 4-(2-hydroxynaphthalen-1-ylazo)benzoic acid (2a)

4-Aminobenzoic acid (**1**) (0.500 g, 3.65 mmol) was dissolved in 25% HCl solution (10.0 mL of hydrochloric acid in 30.0 mL of water) and the mixture was stirred in an ice bath until the reaction temperature reached 0 °C. To such prepared solution, the previously cooled aqueous solution of $NaNO_2$ (0.252 g, 3.65 mmol of $NaNO_2$ in 5.00 mL of dist. water) was added dropwise at 0 °C. The mixture was stirred further for 15 min after the last portion of $NaNO_2$ solution had been added. To the aqueous solution of NaOH (36.5 g, 0.913 mol of NaOH in 20.0 mL of dist. water), in which 2-hydroxynaphthalene (0.526 g, 3.65 mmol) was dissolved, the solution of the previously prepared diazonium salt was added dropwise, keeping the temperature range between –2 and 0 °C. The resulting mixture was stirred for about 1 h in an ice bath and then 2 h at room temperature. The pH value of the total solution was leveled to 6–7 using 10% aqueous solution of sodium bicarbonate. The product was filtered and dried over a vacuum and recrystallized from acetic acid, giving a yield of 65%; mp = 287–288 °C; FT-IR (KBr, ν/cm^{-1}): 3444 (OH + NH), 1677 (C=O, COOH), 1625 (C=O), 1604 (C=C, C_6H_4), 1504 and 1430 (C=N); ^{1}H NMR (400 MHz, DMSO-d_6, δ/ppm): 15.88 (1H, s, NH), 8.47 (1H, d, J= 8.0 Hz, $C_{10}H_6$), 8.06 (2H, d, J= 8.8 Hz, C_6H_4), 7.95 (1H, d, J= 9.6 Hz, $C_{10}H_6$), 7.87 (2H, d, J= 8.8 Hz, C_6H_4), 7.75 (1H, d, J= 7.6 Hz, $C_{10}H_6$), 7.62 (1H, ddd, J= 7.6 Hz; 0.8 Hz, $C_{10}H_6$), 7.48 (1H, ddd, J= 7.4 Hz; 1.2 Hz, $C_{10}H_6$), 6.80 (1H, d, J= 9.6 Hz, $C_{10}H_6$); ^{13}C NMR (100 MHz, DMSO-d_6, δ/ppm): 175.78 (COOH), 167.35 (C=O), 147.01 ($C_{10}H_6$), 142.54 (C_6H_4), 133.20 ($C_{10}H_6$), 131.52 (2C, C_6H_4), 130.60 ($C_{10}H_6$), 130.00 ($C_{10}H_6$), 129.67 ($C_{10}H_6$), 129.58 ($C_{10}H_6$), 128.55 ($C_{10}H_6$), 127.23 ($C_{10}H_6$), 125.85 ($C_{10}H_6$), 122.21 (C_6H_4), 117.91 (2C, C_6H_4).

2.4.1.2. Synthesis of 4-(4-hydroxyphenylazo)benzoic acid (2b)

The same synthetic procedure as the one for compound **2a** was applied: 4-Aminobenzoic acid (0.500 g, 3.65 mmol), 25% aqueous solution of HCl (30.0 mL), $NaNO_2$ (0.250 g, 3.62 mmol) in water (5.00 mL); phenol (0.350 g, 3.72 mmol), NaOH (2.00 g, 0.0500 mol) in 20.0 mL of water. Yield 68%; mp = 258–260 °C; FT-IR (KBr,

ν/cm^{-1}): 3237 (OH), 1688 (C=O, COOH), 1604 (C=C, C_6H_4), 1505 (N=N); ^{1}H NMR (400 MHz, DMSO-d_6, δ/ppm): 11.77 (1H, s, COOH), 8.19 (2H, d, J= 8.4 Hz, C_6H_4), 7.97–7.92 (4H, m, C_6H_4), 7.06 (2H, d, J= 8.8 Hz, C_6H_4); ^{13}C NMR (100 MHz, DMSO-d_6, δ/ppm): 167.32 (COOH), 162.15 (C_6H_4), 155.00 (C_6H_4), 146.77 (C_6H_4), 132.56 (C_6H_4), 131.03 (2C, C_6H_4), 125.79 (2C, C_6H_4), 122.55 (2C, C_6H_4), 116.56 (2C, C_6H_4).

2.4.1.3. Synthesis of 4-[4-(*N*,*N*-dimethylamino)phenylazo]benzoic acid (2c)

The synthetic procedure was the same as the one described for compound **2a**. 4-Aminobenzoic acid (0.500 g, 3.65 mmol), 50% HCl solution (30.0 mL), $NaNO_2$ (0.252 g, 0.365 mmol) in 5.00 mL of water; N,N-dimethylaniline (0.465 mL, 3.67 mmol) in 25% aqueous solution of HCl. Yield 45%; mp = 249–250 °C; FT-IR (KBr, ν/cm^{-1}): 3433 (OH), 1682 (C=O, COOH), 1597 (C=C, C_6H_4), 1521 (N=N); ^{1}H NMR (400 MHz, DMSO-d_6, δ/ppm): 13.17 (1H, s, COOH), 8.15 (2H, d, J= 8.4 Hz, C_6H_4), 7.92–7.89 (4H, m, C_6H_4), 6.91 (2H, d, J= 9.2 Hz, C_6H_4), 3.15 (6H, s, CH_3); ^{13}C NMR (100 MHz, DMSO-d_6, δ/ppm): 167.40 (COOH), 155.51 (C_6H_4), 153.44 (C_6H_4), 144.13 (C_6H_4), 131.40 (C_6H_4), 130.97 (2C, C_6H_4), 125.74 (2C, C_6H_4), 122.20 (2C, C_6H_4), 112.04 (2C, C_6H_4), 40.30 (2C, $N(CH_3)_2$).

2.4.2. Synthesis of 4-arylazocinnamic acids

All of the targeted 4-arylazocinnamic acids were obtained by modified synthetic procedures [14,15,20–24]. FT-IR, ^{1}H NMR, and ^{13}C NMR results of **3A**–**C** correspond to those in the literature [20,23,24].

2.4.2.1. Synthesis of 4-nitrocinnamic acid (3A)

A mixture of 4-nitrobenzaldehyde (**3**) (25.0 g, 165 mmol), sodium acetate (19.7 g, 229 mmol), and acetic anhydride (34.7 g, 340 mmol) was put in a 500-mL round-bottomed flask equipped with a stirrer and a condenser and heated in an oil bath (180 °C). The mixture was held as such for about 13 h, whereby the content of the flask was well stirred. After the reaction product had been obtained, it was cooled slightly and then poured into 300–400 mL of water, after which suction via a Buchner funnel was performed, followed by several rinses with distilled water and a 10% ammonia solution. The solid was again washed with distilled water and taken to drying, giving a yield of 60%; mp = 274–277 °C.

2.4.2.2. Synthesis of methyl 4-nitrocinnamate (3B)

4-Nitrocinnamic acid (**3A**) (13.7 g, 77.3 mmol), anhydrous methanol (350 mL), and sulfuric acid (10.0 mL) were poured into a 500-mL round-bottom flask equipped with a stirrer and a condenser and heated in an oil bath (200 °C). The mixture was energetically stirred and heated for about 8 h. After the reaction had finished (which could be seen by the formation of white crystals by cooling), the excess of methanol was removed via distillation of the mixture. The product, which still contained a significant amount of methanol, was extracted from the mixture using chloroform and a 10% aqueous solution of sodium bicarbonate. The product was recrystallized from ethanol to give a yield of 73%; mp = 98–101 °C.

2.4.2.3. Synthesis of methyl 4-aminocinnamate (3C)

Methyl 4-nitrocinnamate (**3B**) (10.0 g, 48.3 mmol), methanol (210 mL), distilled water (25.0 mL), and ammonium chloride (4.43 g, 82.8 mmol) were put into a 250-mL round-bottom flask equipped with a magnetic stirrer. Zinc dust (31.6 g, 0.483 mol) was added gradually, taking care that the reaction mixture did not overheat. After the whole portion of zinc dust was added, the flask was equipped with a condenser and gradually heated in an oil bath. The reaction mixture was kept at reflux temperature for about 5 h. After the reaction had finished, the product was filtered by suction and then extracted using chloroform and a 10% aqueous solution of sodium bicarbonate. The crude product was recrystallized from diethyl ether to give a yield of 70%; mp = 109–111 °C.

2.4.2.4. Synthesis of methyl 4-(2-hydroxynaphthalen-1-ylazo)cinnamate (4a)

To a solution of methyl 4-aminocinnamate (**3C**) (0.500 g, 2.82 mmol), hydrochloric acid (1.45 mL), and water (100 mL), previously cooled to 0 °C, a clear cooled solution of sodium nitrite (0.950 g, 13.8 mmol) in 10.0 mL of water was added dropwise, maintaining the noted temperature. 2-Hydroxynaphthalene (0.505 g, 3.50 mmol) was dissolved in aqueous NaOH (0.210 g, 5.25 mmol, in 5.00 mL of water) and well stirred until the temperature of the clean solution reached 0 °C. To this solution was added a solution of diazonium salt dropwise, maintaining the temperature at 0 °C. After the whole portion of diazonium salt was added, the mixture was stirred for about 30 min in an ice bath and then for 2 h at room temperature. The product was collected by vacuum filtration and left to dry. Yield 78%; mp = 158–161 °C; FT-IR (KBr, ν/cm^{-1}): 3445 (NH), 1715 (C=O, COOH), 1632 (C=O, $COOCH_3$ + C=C, CH=CH), 1600 (C=C, C_6H_4), 1499 and 1436 (C=N); ^{1}H NMR (400 MHz, DMSO-d_6, δ/ppm): 15.85 (1H, s, NH), 8.50 (1H, d, J= 8.4 Hz, $C_{10}H_6$), 7.94 (1H, d, J= 9.6 Hz, $C_{10}H_6$), 7.88–7.83 (4H, m, C_6H_4), 7.76 (1H, d, J= 7.6, $C_{10}H_6$), 7.70 (1H, d, J= 16.0 Hz, CH=CH), 7.63–7.59 (1H, m, $C_{10}H_6$), 7.49–7.45 (1H, m, $C_{10}H_6$), 6.84 (1H, d, J= 9.2 Hz, $C_{10}H_6$), 6.68 (1H, d, J= 16.0 Hz, CH=CH), 3.75 (3H, s, CH_3); ^{13}C NMR (100 MHz, DMSO-d_6, δ/ppm): 173.21 (C=O, ester), 167.15 (C=O), 145.98 ($C_{10}H_6$), 144.08 (CH=CH), 141.69 (C_6H_4), 133.23 ($C_{10}H_6$), 133.17 ($C_{10}H_6$), 130.48 (2C, C_6H_4), 130.31 ($C_{10}H_6$), 129.83 ($C_{10}H_6$), 129.54 ($C_{10}H_6$), 128.45 ($C_{10}H_6$), 126.86 ($C_{10}H_6$), 125.26 ($C_{10}H_6$), 122.09 ($C_{10}H_6$), 119.01 (2C, C_6H_4), 118.13 (CH=CH), 51.95 (CH_3).

2.4.2.5. Synthesis of methyl 4-(4-hydroxyphenylazo)cinnamate (4b)

Methyl 4-aminocinnamate (**3C**) (0.500 g, 2.82 mmol), hydrochloric acid (0.920 mL), and water (100 mL) were put into a 100-mL beaker equipped with a magnetic stirrer and mixed in an ice bath (0 °C) to complete solution. The aqueous solution of sodium nitrite (0.140 g $NaNO_2$ in 5.00 mL of water), previously well mixed and cooled, was added dropwise. The whole mixture was cooled to 0 °C and added dropwise to the aqueous solution of phenol (0.310 g, 3.29 mmol) in KOH (0.540 g, 9.62 mmol in 25.0 mL of dist. water), recently cooled to 0 °C as well. After the diazotation was carried out, the reaction mixture was further stirred for about 2 h at room temperature. The product was collected by filtration and recrystallized from ethanol and water to give a yield of 54%; mp > 320 °C; FT-IR (KBr, ν/cm^{-1}): 3426 (OH), 1686 (C=O, $COOCH_3$), 1627 (C=C, CH=CH), 1592 (C=C, C_6H_4), 1505 (N=N); ^{1}H NMR (400 MHz, DMSO-d_6, δ/ppm): 10.51 (1H, s, OH), 7.99 (2H, d, J= 8.8 Hz, C_6H_4), 7.92–7.89 (4H, m, C_6H_4), 7.81 (1H, d, J= 16.0 Hz, CH=CH), 7.03 (2H, d, J= 8.8 Hz, C_6H_4), 6.82 (1H, d, J= 16.4 Hz, CH=CH), 3.82 (3H, s, CH_3); ^{13}C NMR (100 MHz, DMSO-d_6, δ/ppm): 167.03 (C=O, $COOCH_3$), 161.85 (C_6H_4), 153.40 (C_6H_4), 145.81 (C_6H_4), 143.99 (CH=CH), 136.32

(C_6H_4), 129.99 (2C, C_6H_4), 125.62 (2C, C_6H_4), 123.04 (2C, C_6H_4), 119.42 (CH=CH), 116.51 (2C, C_6H_4), 52.05 (CH_3).

2.4.2.6. Synthesis of methyl 4-[4-(*N*,*N*-dimethyl)phenylazo]cinnamate (4c)

N,*N*-Dimethylaniline (0.360 mL, 2.82 mmol) was dissolved in a 30% aqueous solution of hydrochloric acid (25.0 mL) and left stirring in an ice bath until the temperature reached 0 °C. At this temperature, a previously made and cooled solution of diazonium salt was added dropwise, keeping the temperature within a range of –2 to 0 °C. Diazonium salt was prepared in the same manner as for compounds **4a** and **4b**. The crude product, collected by filtration, was recrystallized from DMSO to give a yield of 44%; mp = 187–190 °C; FT-IR (KBr, ν/cm^{-1}): 1703 (C=O, $COOCH_3$), 1631 (C=C, CH=CH), 1601 (C=C, C_6H_4), 1518 (N=N); ^{1}H NMR (400 MHz, DMSO-d_6, δ/ppm): 7.88 (2H, d, J= 8.4 Hz, C_6H_4), 7.83–7.79 (4H, m, C_6H_4), 7.73 (1H, d, J= 16.0 Hz, CH=CH), 6.85 (2H, d, J= 8.8 Hz, C_6H_4), 6.72 (1H, d, J= 16.0 Hz, CH=CH), 3.75 (3H, s, CH_3), 3.08 (6H, s, $N(CH_3)_2$); ^{13}C NMR (100 MHz, DMSO-d_6, δ/ppm): 167.09 (C=O, $COOCH_3$), 153.93 (C_6H_4), 153.29 (C_6H_4), 144.18 (C_6H_4), 143.20 (CH=CH), 135.37 (C_6H_4), 129.94 (2C, C_6H_4), 125.56 (2C, C_6H_4), 122.70 (2C, C_6H_4), 118.83 (CH=CH), 112.08 (2C, C_6H_4), 51.96 (CH_3, $COOCH_3$), 40.32 (2C, $N(CH_3)_2$).

2.4.2.7. Synthesis of 4-(4-hydroxyphenylazo)cinnamic acid (5a)

Methyl 4-(4'-hydroxyphenylazo)cinnamate (**4a**) (55.0 mg, 0.195 mmol) was added in a round-bottom flask along with previously dissolved KOH (5.05 g, 90.0 mmol) in ethanol (30.0 mL) and well mixed at reflux temperature for about 13 h. After the hydrolysis was done, which was monitored on TLC (CH_2Cl_2/MeOH = 19/1), the reaction mixture was poured into 100 mL of water, acidified, left overnight, and after that filtered over a vacuum. The crude product was recrystallized from acetic acid to give a yield of 72%; mp = 285–287 °C; FT-IR (KBr, ν/cm^{-1}): 3434 (OH + NH), 1675 (C=O, COOH), 1625 (C=C, CH=CH + C=O), 1600 (C=C, C_6H_4), 1501 and 1431 (C=N); ^{1}H NMR (400 MHz, DMSO-d_6, δ/ppm): 15.84 (1H, s, NH), 12.42 (1H, s, COOH), 8.48 (1H, d, J= 8.0 Hz, $C_{10}H_6$), 7.93 (1H, d, J= 9.6 Hz, $C_{10}H_6$), 7.83 (4H, s, C_6H_4), 7.74 (1H, d, J= 8.0 Hz, $C_{10}H_6$), 7.63 (1H, d, J= 16.0 Hz, CH=CH), 7.60 (1H, t, J= 7.6 Hz, $C_{10}H_6$), 7.46 (1H, t, J= 7.4 Hz, $C_{10}H_6$), 6.84 (1H, d, J= 9.6 Hz, $C_{10}H_6$), 6.57 (1H, d, J= 16.0 Hz, CH=CH); ^{13}C NMR (100 MHz, DMSO-d_6, δ/ppm): 172.71 (COOH), 168.03 (C=O), 145.85 ($C_{10}H_6$), 143.47 (CH=CH), 141.52 (C_6H_4), 133.59 ($C_{10}H_6$), 133.16 ($C_{10}H_6$), 130.28 (2C, C_6H_4), 130.23 ($C_{10}H_6$), 129.78 ($C_{10}H_6$), 129.50 ($C_{10}H_6$), 128.42 ($C_{10}H_6$), 126.78 ($C_{10}H_6$), 125.13 ($C_{10}H_6$), 122.03 ($C_{10}H_6$), 119.65 (CH=CH), 119.09 (2C, C_6H_4).

2.4.2.8. Synthesis of 4-(2-hydroxynaphhalen-1-ylazo)cinnamic acid (5b)

The procedure for obtaining 4-(2-hydroxynaphthalene-1-ylazo)cinnamic acid was the same as that for obtaining compound **5a**. Quantities of reactives were: 50.0 mg (0.156 mmol) of methyl 4-(2-hydroxynaphthalen-1-ylazo)cinnamate (**4b**), KOH (5.05 g, 90.0 mmol), and ethanol (30.0 mL). Yield 59%; mp = 246–249 °C; FT-IR (KBr, ν/cm^{-1}): 3403 (OH), 3238 (OH, COOH), 1692 (C=O, COOH), 1625 (C=C, CH=CH), 1588 (C=C, C_6H_4), 1503 (N=N); ^{1}H NMR (400 MHz, DMSO-d_6, δ/ppm): 12.34 (1H, s, COOH), 10.55 (1H, s, OH), 7.96 (2H, d, J= 8.4 Hz, C_6H_4), 7.92–7.89 (4H, m, C_6H_4), 7.74 (1H, d, J= 16.0 Hz, CH=CH), 7.05 (2H, d, J= 8.8 Hz, C_6H_4), 6.71 (1H, d, J= 16.0 Hz, CH=CH); ^{13}C NMR (100 MHz, DMSO-d_6, δ/ppm):

172.45 (COOH), 167.88 (C_6H_4), 153.28 (C_6H_4), 145.81 (C_6H_4), 143.35 (CH=CH), 136.59 (C_6H_4), 129.79 (2C, C_6H_4), 125.55 (2C, C_6H_4), 123.04 (2C, C_6H_4), 120.91 (CH=CH), 116.52 (2C, C_6H_4).

2.4.2.9. Synthesis of 4-(4-(*N*,*N*-dimethylamino)phenylazo)cinnamic acid (5c)

For obtaining 4-[4'-(N,N-dimethylamino)phenyl-azo]cinnamic acid a similar synthetic procedure as the one for compound **5a** was performed. A mixture of methyl 4-[4'-(N,N-dimethyl)phenylazo]cinnamate (**4c**, 50.0 mg, 0.161 mmol), KOH (5.05 g, 90.0 mmol), and ethanol (35.0 mL) was poured into a round-bottom flask and vigorously stirred under reflux for 21 h. The reaction was monitored by TLC. The crude product was recrystallized from ethanol and water to give a yield of 43%; mp $>$ 320 °C; FT-IR (KBr, ν/cm^{-1}): 1674 (C=O, COOH), 1622 (C=C, CH=CH), 1598 (C=C, C_6H_4), 1518 (N=N); ^{1}H NMR (400 MHz, DMSO-d_6, δ/ppm): 7.89 (2H, d, J= 8.8 Hz C_6H_4), 7.86 (4H, s, C_6H_4), 7.59 (1H, d, J= 16.0 Hz, CH=CH), 6.93 (2H, d, J= 9.2 Hz, C_6H_4), 6.73 (1H, d, J= 16.0 Hz, CH=CH), 3.16 (6H, s, N(CH_3)$_2$); ^{13}C NMR (100 MHz, DMSO-d_6, δ/ppm): 168.41 (COOH), 153.50 (C_6H_4), 153.18 (C_6H_4), 143.17 (C_6H_4), 142.11 (CH=CH), 136.14 (C_6H_4), 129.50 (2C, C_6H_4), 125.48 (2C, C_6H_4), 122.70 (2C, C_6H_4), 122.24 (CH=CH), 112.06 (2C, C_6H_4), 40.32 (2C, N(CH_3)$_2$).

3. Results and discussion

3.1. Tautomerism and solvatochromism of the dyes

Four of the six synthesized azo dye molecules theoretically exhibit azo-hydrazone tautomerism, due to the presence of the hydroxy group in *ortho*- (**2a** and **5a**) and *para*- (**2b** and **5b**) positions to the azo bridge (Figure 2).

According to FT-IR data (Section 2), strong, wide bands for **2a** and **5a** can be noted at 3444 and 3434 cm^{-1}, which can be attributed to mutual –NH hydrazone and –OH carboxy stretchings. On the other hand, wide bands at 3237 and 3238 cm^{-1} for **2b** and **5b**, respectively, originate from –OH stretchings of a carboxy group, whereas, for **5b**, a band at 3403 cm^{-1} is ascribed to –OH stretching of a phenolic group. The bands at 1500–1700 cm^{-1} are assigned to the stretching vibrations of C=O and C=N groups of dye molecules **2a** and **5a**. The existence of these bands in the FT-IR spectra confirms the hydrazone structure of dye molecules and supports the literature data [25,26]. Moreover, compounds **2b** and **5b** show the absence of stretching of the second carbonyl band, which would have originated from the noncarboxylic C=O group in the 1630–1700 cm^{-1} domain [27,28], if the mentioned azo dye molecules had been found as hydrazone tautomers. The bands at 1505 and 1503 cm^{-1} are assigned to –N=N– stretching vibrations for **2b** and **5b**, respectively [29,30].

The ^{1}H NMR spectra of compounds **2a** and **5a** show solitary peaks at 15.93 and 15.84 ppm, respectively, originating from the –NH group of hydrazone tautomer. Dye molecules **2b** and **5b** show no lone peaks in this region and it can be assumed that they exist only as azo tautomers. Signals of peaks at 173.22 and 172.71 ppm in the ^{13}C NMR spectra for molecules of **2a** and **5a**, respectively, are ascribed to a carbonyl C atom present in hydrazone form. The ^{13}C NMR spectra of compounds **2b** and **5b** do not exhibit these peaks, supporting the fact that in these dye molecules an azo tautomer is dominant. These data are consistent with those given in the literature [31–33].

In **2a** and **5a**, there is a strong intramolecular hydrogen bond in both tautomers, forming a six-membered pseudo ring within the molecules. The factor serving in favor of the hydrazone form is the fact that the

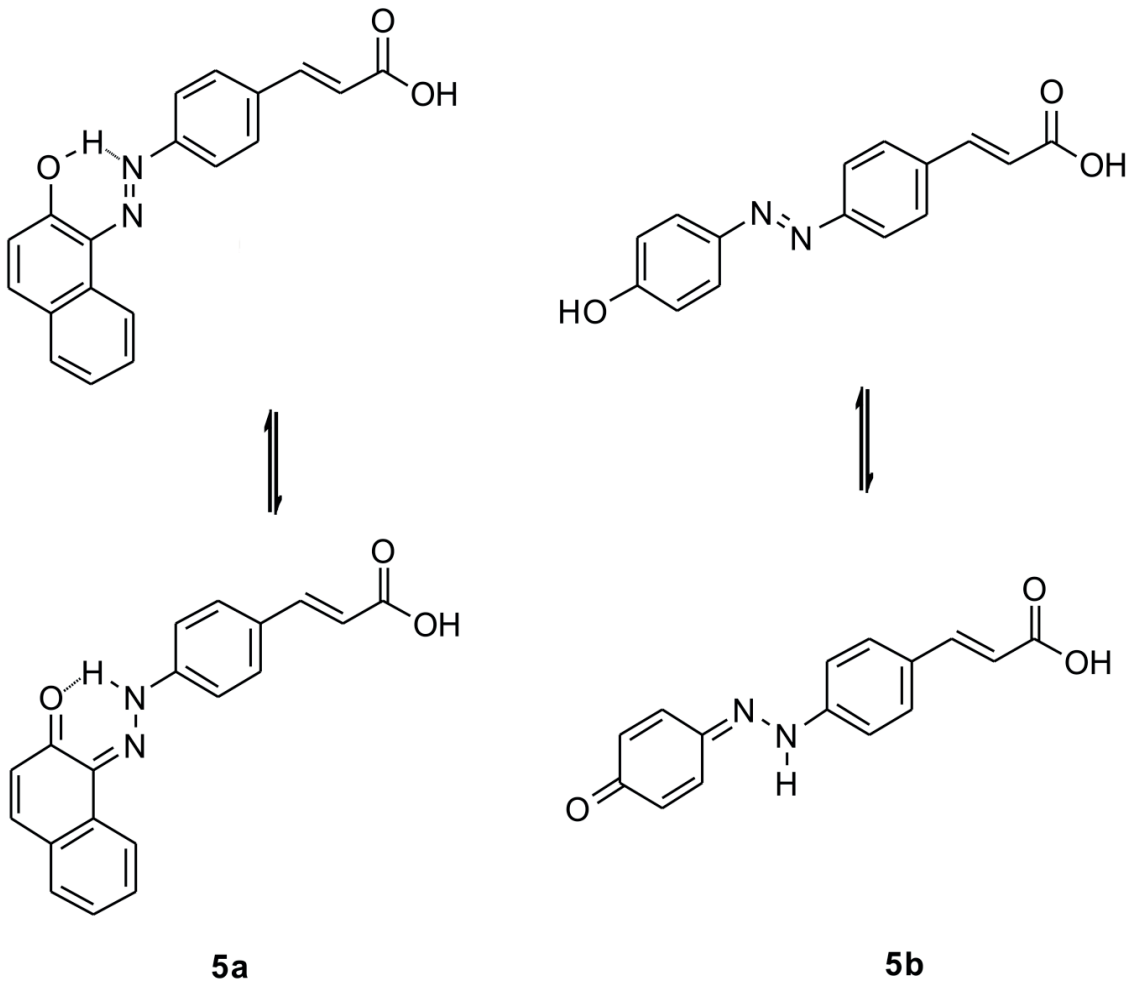

Figure 2. Azo-hydrazone tautomerism in **5a** and **5b** (similar scheme can be depicted for compounds **2a** and **2b**).

intramolecular hydrogen bond is stronger than in the azo form due to higher bond polarities (Figure 2) [34–36]. The dominance of the azo form in phenylazo dyes **2b** and **5b** may be attributed to the loss of the aromatic character of the ring in the hydrazone form, while in the case of hydroxyazonaphthalene dyes (**2a** and **5a**) this loss is limited to only one of the naphthalene rings. In light of this, the tautomers of **2a** and **5a** are expected to be of similar stability and thus the equilibrium between azo and hydrazone forms is highly dependent on the microenvironment of the particular tautomers [37,38].

Three solvents of different properties: ethanol, DMSO, and acetonitrile, were used to investigate the solvatochromism of the six selected azo dye molecules (Figure 3). The experimentally obtained absorption maxima, as well as molar extinction coefficient values, are given in Table 1.

It can be presumed from Figure 3 that strong absorption peaks of compounds in all three solvents arise from $\pi-\pi*$ transitions between two corresponding aryl rings. High-energy bands originate from $n-\pi*$ electron transitions between phenyl rings of benzoic/cinnamic acid and the bridging azo unit [37,38]. It can be noted that all compounds derived from cinnamic acid (compounds **5a**–**c**) are bathochromically shifted with respect to those derived from benzoic acid (compounds **2a**–**c**, respectively) due to extended conjugation. Molecule

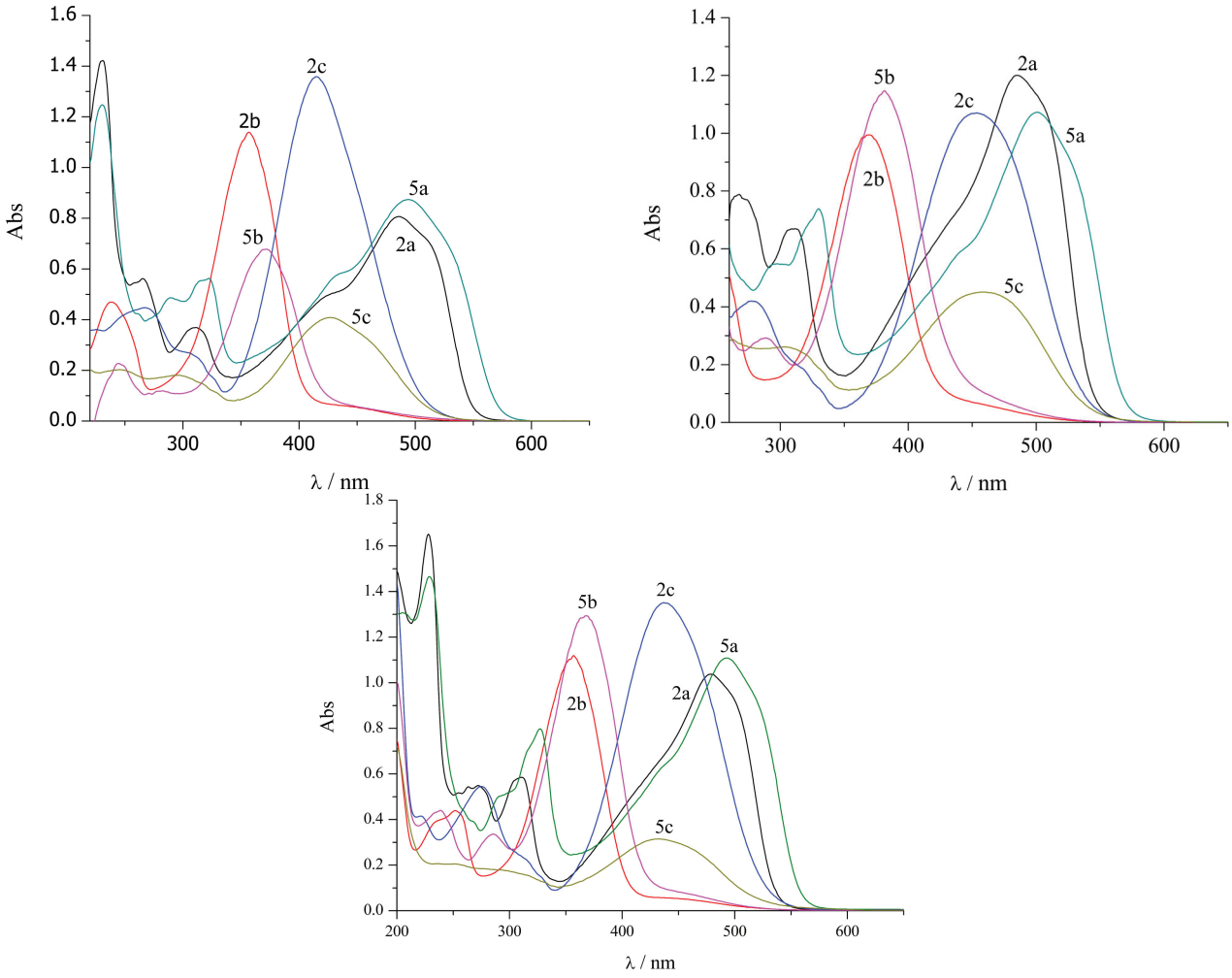

Figure 3. UV-Vis absorption spectra of the synthesized dye molecules in: a) ethanol, b) DMSO, and c) acetonitrile.

Table 1. Experimentally determined values for main absorption maxima and extinction coefficents for six synthesized azo dyes in three different solvents.

Compound	EtOH		DMSO		CH_3CN	
	λ_{max}, [nm]	ε, [m^2/mol]	λ_{max}, [nm]	ε, [m^2/mol]	λ_{max}, [nm]	ε, [m^2/mol]
2a	486	1612	485	2400	479	2074
2b	357	2278	370	1988	357	2238
2c	415	2716	453	2140	437	2702
5a	494	1748	501	2146	492	2216
5b	372	1356	381	2294	369	2586
5c	429	818	458	902	433	620

2a is bathochromically shifted with respect to **2b** and **2c** due to the better electron-donating effect of the 2-hydroxynaphthalene unit. There is an influence of intramolecular stabilization present in azo dye **2a**, which also contributes to the red-shifting of the same. The same trend can be noted within the **5a**–**c** series. It can be

noted that the UV-Vis spectra of **2a** and **5a** in all solvents have shoulders on both the lower and higher energy sides, which is the consequence of azo-hydrazone tautomerism in these solutions (Figure 2).

Hydrochloric acid and solid sodium hydroxide were added dropwise to the ethanolic solutions of dye molecules **2a** and **5a** in order to establish the influence of an acid/base on the equilibrium (Figures 4a and 4b).

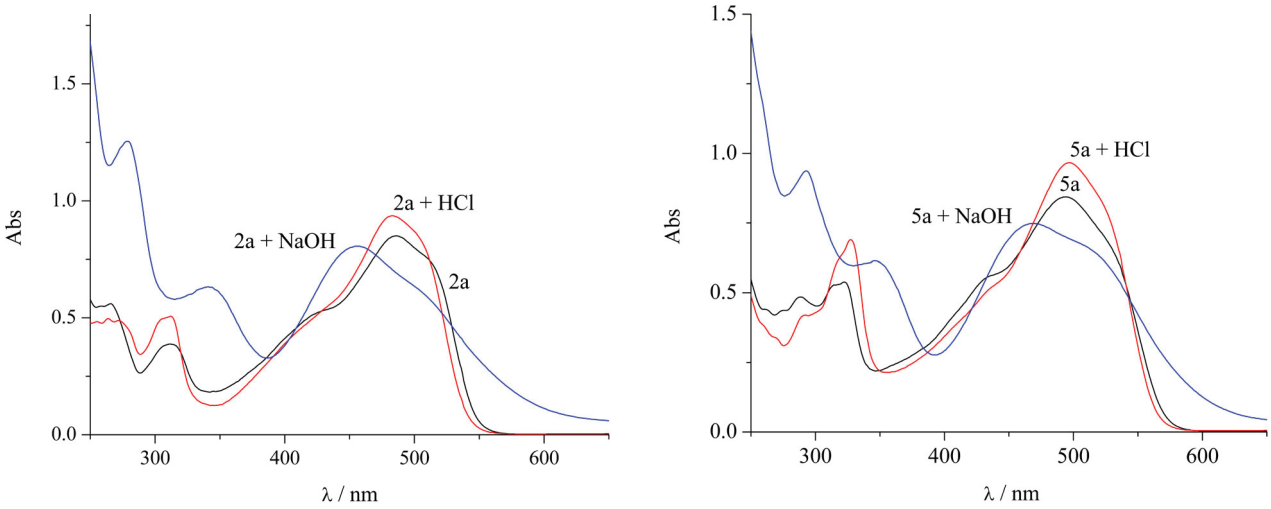

Figure 4. Influence of HCl and NaOH added on absorption maximum of a) **2a** and b) **5a**.

It can be noted that the addition of acid only hyperchromically shifted the absorbance maxima of both **2a** and **5a** dye molecules. This is the indicator of hydrazone tautomer dominance in solution since it dominates at lower pH [39]. On the other hand, the addition of NaOH stretched the peaks of both **2a** and **5a** molecules; shoulders on the higher energy side of both molecules disappeared, while the main peaks as well as the peaks on the lower energy side were hypsochromically shifted. Two new main absorption peaks emerged, centered at 456 nm and 469 nm for **2a** and **5a**, respectively, while the peaks from the higher wavelength shifted to 494 nm for **2a** and 500 nm for **5a**. Moreover, the intensity of the very same absorption peaks decreased (hypochromic shift occurred). This phenomenon in the alkaline medium could be an indicator of deionization, i.e. the existence of deprotonated species of both molecules **2a** and **5a** as presented in Figure 5 [33].

3.2. Photovoltaic measurements and computational study

3.2.1. DSSC operational performance simulation

Extensive work has been performed so far on the design and synthesis of the optimal azo dye molecule with D–π–A structure since this type of structure has been shown as one of the most prominent molecular structures for efficient photovoltaic performance [1,4,5,8]. Table 2 summarizes experimentally obtained data of structural analogues of the investigated azo dyes in this paper bearing the same/similar backbone.

The J_{SC}–V_{OC} curves of DSSCs based on six azo dye molecules containing benzoic (**2a**–**c**) and cinnamic acid moiety (**5a**–**c**), along with di-tetrabutylammonium cis-bis(isothiocyanato)bis(2,2'-bipyridyl-4,4'-dicarboxylato)ruthenium(II) dye (**N719**) as the referent one, are presented in Figure 6. The rest of the DSSCs'key operating parameters, such as maximum power (P_{max}), fill factor (ff), and conversion efficiency (η) are calculated by Eqs. (1) and (2) and presented in Table 3 [41,42].

The shape of the J_{SC}–V_{OC} curve is determined by ff, which basically represents the ratio of theoretically

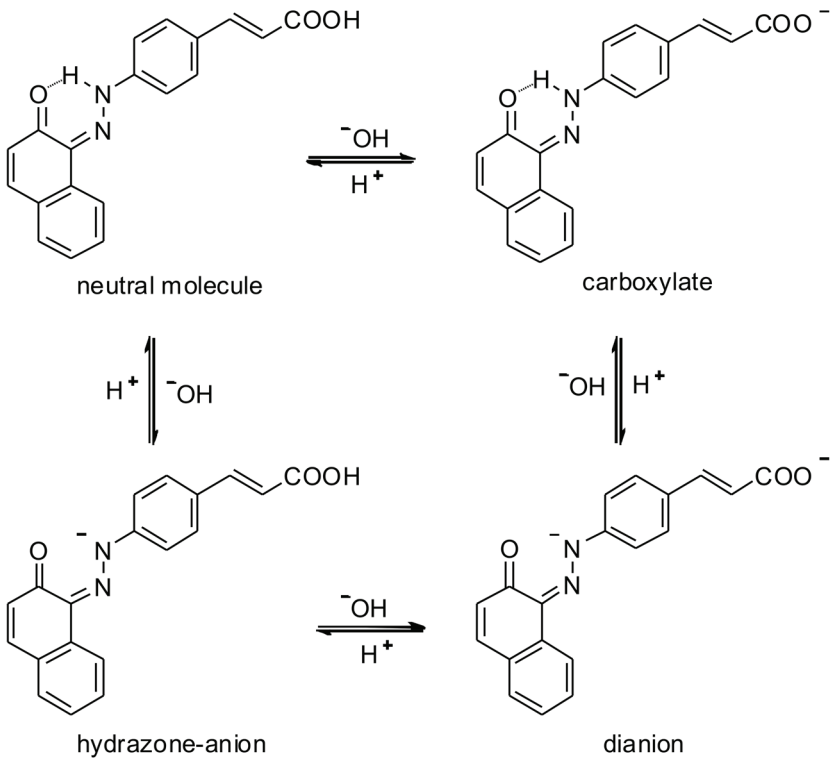

Figure 5. Possible anion/dianion formation in ethanolic solution of **5a** hydrazone tautomer in alkaline medium (similar scheme can be presented for **2a**).

Table 2. Reported data for some azo dye molecules.

Comp.	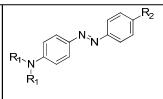					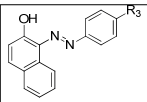			
	R_1 = CH_3 R_2 = COOH [4]		R_1 = CH_3 R_2= COOH [8]		R_1 = CH_2CH_3 R_2= NO_2 [40]	R_3 = COOH [1]	R_3 = CH=CHCOOH [1]	R_3 = COOH [5]	R_3 = CH=CHCOOH [5]
E_{HOMO}, [eV]	*cis-*	–5.76	*cis-*	–5.30	–3.20	–8.792	–1.474	–6.05	–5.93
	trans-	–5.77	*trans-*	–2.16					
E_{LUMO}, [eV]	*cis-*	–2.30	*cis-*	–5.28	–5.60	–8.727	–1.502	–2.91	–2.95
	trans-	–2.63	*trans-*	–1.91					
$E_{CB}(TiO_2)$, [eV]	–4.10		–4.04		–4.94	/		–3.98	
$E_{I-/I3-}$, [eV]	–4.80		–4.94		–4.94	/		–4.90	
Package	Gaussian 03		Gaussian 09		Gaussian 09	MOPAC7		Gaussian 09	
Optimiz. method/ set	PBE0/6-31+G**		B3LYP and 3-21g*/6-31g(d,p)		B3LYP and 6-31+g(d,p)	/		B3LYP/6-31G(d,p) and TD-B3LYP/6-311G(d,p) methods	
Solvent/ Medium	DMSO		Vacuum		/	/		/	

obtainable maximum power and power achieved upon illumination of the DSSCs. The value of ff is on a scale from 0 to 1, referring to total to no electrical and electrochemical losses occurring during the DSSC operation, respectively. A higher value of ff means that the J_{SC}–V_{OC} curve will take a more rectangular form. This parameter is theoretically presented in Eq. (1):

$$ff = \frac{J_{mp} \times V_{mp}}{J_{SC} \times V_{OC}}, \tag{1}$$

where J_{mp} [mA/cm^2] stands for short-current density at maximum power and V_{mp} [V] is voltage at maximum power.

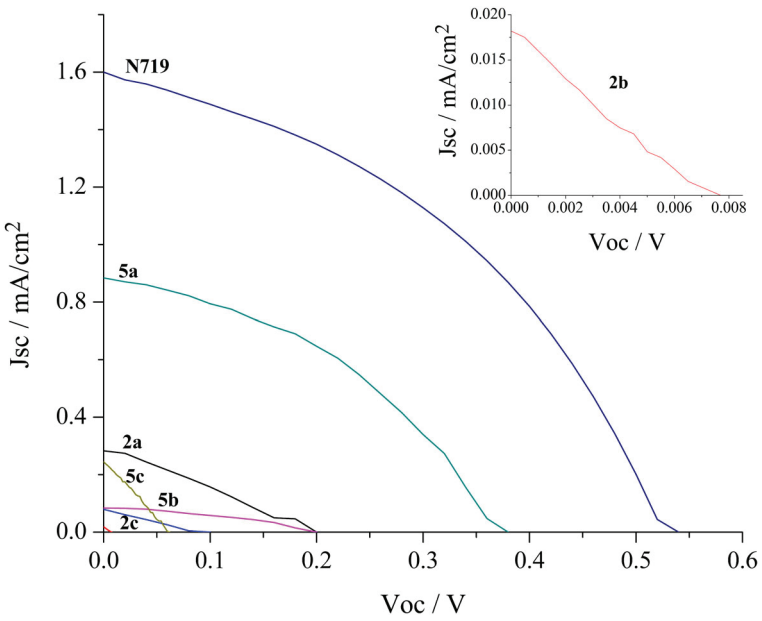

Figure 6. Short-current density-voltage curves of DSSCs of six targeted azo dyes and N719 dye as a referent one.

Table 3. DSSC main parameter features for six azo dyes synthesized in this paper.

Compound	J_{SC} [mA/cm^2]	V_{OC} [mV]	ff	Relative efficiency (η) vs. N719 [%]
N719	1.6	540	0.4	100
2a	0.283	200	0.28	4.57
2b	0.0182	7.7	0.22	0.00886
2c	0.0794	100	0.22	0.5
5a	0.884	380	0.4	40
5b	0.0839	200	0.37	1.77
5c	0.245	62	0.28	1.22

Total solar cell efficiency, i.e. energy-conversion efficiency, as one of the main indicators of operational quality of DSSCs, can be calculated from Eq. (2):

$$\eta = \frac{P_{max}}{P_{in}} = \frac{J_{SC} \times V_{OC} \times ff}{P_{in}}, \tag{2}$$

where P_{in} is the power of incident light (100 mW/cm^2 at AM 1.5).

Values of energy-conversion efficiencies of the six synthesized azo dye molecules are expressed in percentages related to the Ru-complex dye (**N719**), which is marked here as a compound with high energy-conversion efficiency [43].

Dye molecules **2a** and **5a** showed a satisfactory yield of short-current densities, bearing in mind the high potency of **N719**. Owing to a superior electron-donating effect of the 2-hydroxynaphthalene moiety, combined with intramolecular stabilization through hydrogen bonding, these molecules will be considered substrates in the further investigation for DSSC application.

3.2.2. DFT simulation analysis

For a better comprehension of electron charge transfer in the six synthesized azo dye molecules upon excitation, DFT analysis was performed. Figure 7 shows electron distribution in the ground and excited states of a particular azo dye molecule. It can be noted that frontier molecular orbitals (FMOs), highest occupied molecular orbitals (HOMOs), and lowest unoccupied molecular orbitals (LUMOs) are spread over entire molecules in both series, **2a**–**c** and **5a**–**c**. The HOMOs are mainly located at hydroxynaphthyl (**2a** and **5a**), hydroxyphenyl (**2b** and **5b**), and N,N-dimethylaniline ring (**2c** and **5c**), while the LUMOs are diffused over benzoic acid, i.e. cinnamic acid moiety of the molecules. According to this, it can be concluded that, upon excitation, electron density shifts from the electron-donor part of an individual molecule toward the electron-acceptor moiety of the same.

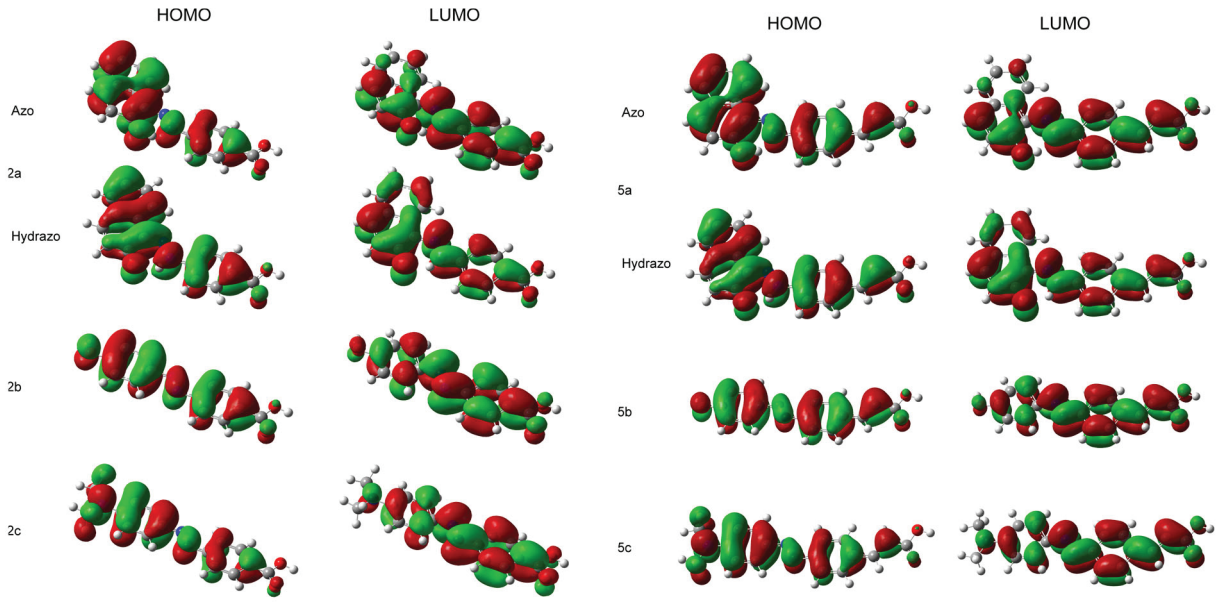

Figure 7. Distribution of frontier molecular orbitals (HOMO–LUMO) of individual azo dye molecules.

As it was mentioned earlier, a photosensitizer has to fulfill several basic conditions to become valid and hence potent. For optimal electron injection, the LUMO energy level of the selected dye molecule must be higher than that the energy level of the conduction band (CB) of TiO_2 (around –4.00 eV). On the other hand, the HOMO energy level must be lower than the energy value of I^-/I_3^- redox potential (around –4.80 eV) in order for rapid reduction of the oxidized dye molecule to occur [4].

Figure 8 depicts the excitation energies of the selected azo dye molecules, calculated by B3LYP method in a vacuum. It can be seen that all HOMO–LUMO energy gaps are within the range of roughly 2.90–3.60 eV, where all LUMO–CB of TiO_2 energy gap values are sufficient for generating enough driving force for effective electron injection. In the same manner, all HOMO energy levels have lower values than I^-/I_3^- redox couple level, which is crucial for the regeneration of the oxidized dye molecule and efficient charge separation. Within the **2a**–**c** series, molecule **2a** has the lowest value of HOMO–LUMO energy gap, which is 3.01 eV for azo and 2.99 eV for hydrazone tautomer (Figure 8). This datum is consistent with the fact that the absorbance maximum of this molecule shows a bathochromic shift compared to the other two molecules within this series, **2b** and **2c** (Figure 3). Furthermore, molecule **2c** has a slight increase in the energy gap value (3.08 eV). This can be attributed to a lower electron-donating effect of the N,N-dimethylamino group compared to the 2-hydroxynaphthalene ring.

Azo dye molecule **2b** has the highest HOMO–LUMO energy gap value (3.57 eV), which is probably due to the least electron-donating effect of the –OH group compared to the other two electron-donating moieties of the selected compounds within the **2a**–**c** series. The same trend can be seen within the **5a**–**c** series, wherein dye molecule **5a** has the lowest energy gap value (2.88 and 2.84 eV for azo and hydrazone tautomer, respectively), followed by **5c** (2.91 eV) and **5b** (3.31 eV). It can be noted that molecules from the **5a**–**c** series have lower HOMO–LUMO gap values compared to those from the **2a**–**c** series, which can be attributed to the extended conjugation in the substructure of cinnamic acid.

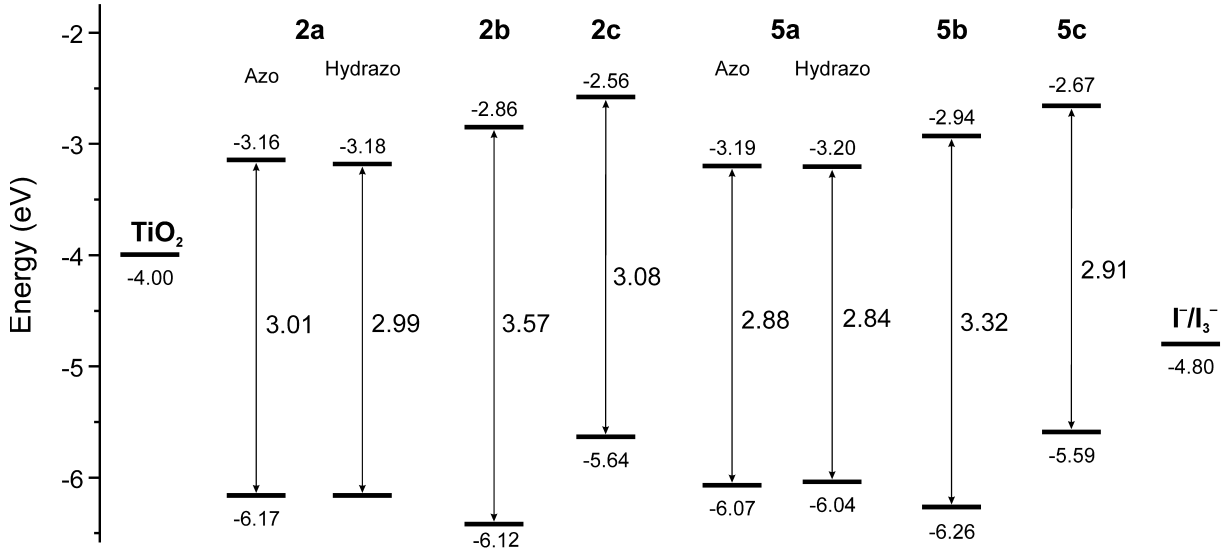

Figure 8. Molecular orbital energy level diagram (eV) of the synthesized azo dyes based on benzoic (**2a**–**c**) and cinnamic acid (**5a**–**c**).

3.2.3. Other DFT simulation results

The additional DFT analysis is summarized in Tables 4 and 5. Hereby, several calculated data for parameters such as maximum absorption wavelength ($\lambda_{\max}$), excitation energy (E_x), oscillator strengths (f), molecular orbital contribution for excitation (MO), light harvesting efficiency (LHE), transferred charge, (q^{CT}, e^-), charge transfer distance, (d^{CT}), H and t indices in Å, and overlap integral are additionally computed for selected azo dye molecules using Gaussian 09 at the TD-CPCM-M06-2X/6-311++G(d,p) level.

3.2.4. Correlation between the HOMO–LUMO energy gap (ΔE), $\lambda_{\max}$, and J*sc*

Supplemental information for quantum chemical calculation analysis from section 3.2.2. can be obtained from the next correlation. Figure 9 depicts the dependence of experimentally obtained data for the HOMO–LUMO energy gap (ΔE) and a) short-circuit current densities (J_{SC}) and b) $\lambda_{\max}$ of the six synthesized azo dye molecules. The HOMO–LUMO energy gap is closely related to the absorption maximum of a particular molecule; the more the compound is red-shifted in the UV-Vis spectrum the lower the HOMO–LUMO energy gap of that molecule will be (less energy will be needed than for the electron excitation after photon has been absorbed by molecule) [44]. In relation to that, by extending the π-conjugation of the particular molecule, the excitation energy will be decreased as well and thus a bathochromic shift will occur. Lowering of the HOMO–LUMO

Table 4. Computed λ_{max}, E_x, f, MO, and LHE of six synthesized azo dyes at the TD-CPCM-M06-2X/6-311++G(d,p) level.

Dye	Tautomer	State	E_x [eV]	λ_{max} [nm]	MO contribution	f	LHE
2a	Azo	S0 → S2	3.12	397.6	H → L (96%)	0.73	0.81
	Hydrazo	S0 → S1	3.00	413.3	H → L (98%)	0.73	0.82
2b		S0 → S2	3.69	336.1	H → L (95%)	1.12	0.92
2c		S0 → S2	3.11	398.9	H → L (94%) H → L+1 (2%)	1.26	0.94
5a	Azo	S0 → S2	3.04	408.1	H → L (94%)	1.03	0.91
	Hydrazo	S0 → S1	2.88	430.0	H → L (96%)	1.00	0.90
5b		S0 → S2	3.51	353.1	H → L (94%) H-2 → L+1 (2%)	1.51	0.97
5c		S0 → S2	3.02	410.0	H → L (90%) H → L+1 (5%)	1.55	0.97

Table 5. Computed q^{CT}, d^{CT}, H, and t indexes in Å and overlap integral of six synthesized azo dyes at the TD-CPCM-M06-2X/6-311++G(d,p) level.

Dye	Tautomer	State	q^{CT}	d^{CT}	H	t	Overlap
2a	Azo	S0 → S2	0.54	2.44	3.25	1.42	0.88
	Hydrazo	S0 → S1	0.47	1.04	3.20	2.24	0.96
2b	Azo	S0 → S2	0.56	2.66	3.20	1.31	0.89
2c	Azo	S0 → S2	0.66	3.74	3.62	1.48	0.85
5a	Azo	S0 → S2	0.52	2.18	3.58	1.68	0.91
	Hydrazo	S0 → S1	0.49	1.18	3.53	2.40	0.97
5b	Azo	S0 → S2	0.52	2.07	3.80	1.94	0.95
5c	Azo	S0 → S2	0.65	3.96	4.09	1.34	0.87

energy gap causes a decrease in the LUMO (dye)–CB (TiO_2) gap, resulting in a quicker electron injection. Furthermore, the decrease in the HOMO–LUMO gap lowers the gap between the HOMO of the dye and the I^-/I_3^- redox couple plateau, thus increasing the reduction rate of the oxidized dye molecule from the redox couple. Both phenomena affect the higher values of a short-circuit current and therefore conversion efficiency of DSSCs [45].

From Figure 9 it can be observed that molecules **5a**–**c** possess lower values of ΔE and hence higher values of both λ_{max} and J_{SC} with respect to the corresponding compound with the same electron-donating group from series **2a**–**c**. As it was explained above, this stems from the fact that extended conjugation, provided by the cinnamic acid moiety in **5a**–**c**, red-shifts the absorbance maxima of the particular molecule, thus resulting in lower excitation energy and hence higher values of generated short-circuit current upon illumination of the molecules. Owing to the greater electron-donating effect of the 2-hydroxynaphthalene unit compared to –$N(CH_3)_2$ and –OH functional groups in **5c** and **5b**, respectively, as well as additional stabilization due to the intramolecular hydrogen bond, azo dye molecule **5a** is red-shifted with respect to other molecules within this series. This results in lower values of ΔE and higher values of J_{SC} with respect to **5b** and **5c**. In the same manner, the better electron-donating effect of the N,N-dimethylamino group over a hydroxy group provides lower values of ΔE for **5c** over **5b**. The same trend can be noted within the **2a**–**c** series.

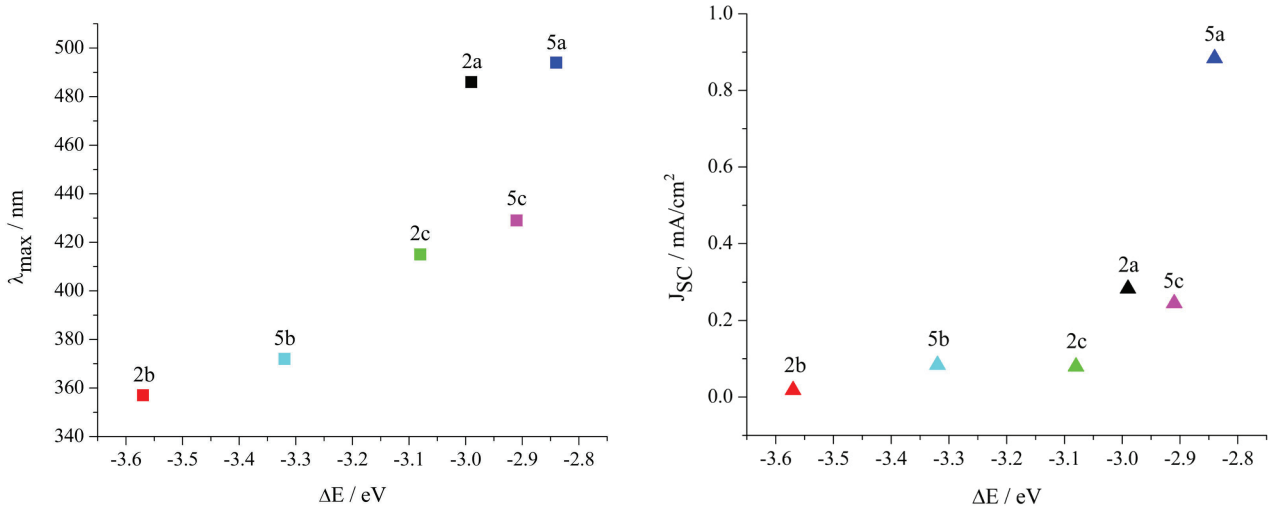

Figure 9. Correlation between HOMO–LUMO energy gap (ΔE) vs. a) short-circuit current density (J_{SC}) and b) λ_{max}.

3.2.5. LUMO orbital energy vs. short-circuit current investigation

As a continuation of the previous discussion, a correlation of LUMO orbital energy values (E_{LUMO}) with J_{SC} values of the synthesized molecules (Figure 10) can be made. As mentioned before, an energy level coupling between the LUMO of the particular molecule and the CB of TiO_2 is essential for optimum electron injection, and hence for solar cell performance [45]. According to that, a lower LUMO energy level should provide better (quicker) electron injection to the CB of TiO_2, since the LUMO–CB energy gap, in that case, will be lower and hence able to provide better electronic communication between these two energy plateaus [45]. As it can be noted from Figure 10, dye molecules **2a** and **5a** yielded the highest values of J_{SC}, which can be attributed to the fact that they possess the lowest values of E_{LUMO}. By comparing the compounds within the series, compound **2a** possesses the lowest value of E_{LUMO} (followed by **2b** and **2c**, respectively), which is reflected in the highest J_{SC}. A similar trend can be noted within the **5a**–**c** series. On the other hand, by comparing molecules with the same electron-donating group from different series, it can be seen that molecules with extended conjugation (**5a**–**c**) have lower values of E_{LUMO} and hence higher values of J_{SC} with respect to those delivered from benzoic acid (**2a**–**c**).

4. Conclusion

The replacement of the benzoic acid moiety with the cinnamic acid moiety effectively extends the π-conjugation within the molecules, thus reducing the HOMO–LUMO gap of these chromophores and shifting the absorption maxima to higher wavelengths. The introduction of an electron-donating substituent has a similar effect, by which bathochromic shift depends on the electron-donating aptitude of individual functional groups and therefore the amount of generated J_{SC}. Hydrazone tautomers of (2-hydroxynaphthaleneazo)benzoic acid (**2a**) and (2-hydroxynaphthaleneazo)cinnamic acid (**5a**) are red-shifted with respect to the other azo dye molecules due to extended π-conjugation in the backbone of the molecule as well as additional stabilization provided by hydrogen bonding between the azo bridge and (the oxygen atom of) the naphthalene ring, which resulted in a higher yield of J_{SC}. It is shown that the amount of generated photocurrent depends on the HOMO–LUMO energy gap as well. Within the series of selected azo dye molecules, it is found that a larger amount of J_{SC} will

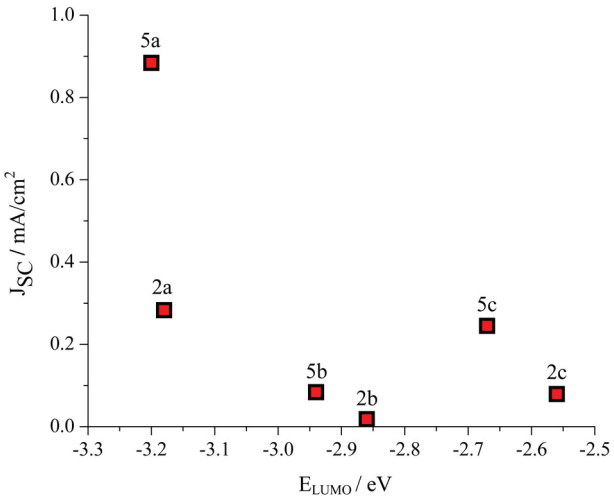

Figure 10. Correlation between LUMO orbital energies (E_{LUMO}) and short-current densities (J_{SC}) of six synthesized azo dye molecules.

be generated if the HOMO–LUMO energy gap is lower, which is determined by the stability of the molecule and the electron-donating effect of the individual functional group. Thus, it is shown that the amount of generated J_{SC} decreases in a series: **5a** > **5c** > **5b** and **2a** > **2c** > **2b**. On the other hand, by comparing molecules from different series with the same electron-donating group, it is concluded that molecules with the cinnamic acid moiety generate higher short-circuit currents with respect to those that contain the benzoic acid moiety. This feature can be attributed to the fact that extended conjugation lowers the HOMO–LUMO gap, which contributes to higher J_{SC} generation due to better electronic communication between energetic levels of titania, dye molecule, and electrolyte. In general, the J_{SC} values obtained for compounds bearing the cinnamic acid moiety (**5a**–**c**) are higher than those of the corresponding compounds containing the benzoic acid moiety (**2a**–**c**).

Acknowledgment

The work was supported by the Ministry of Education, Science and Technological Development of the Republic of Serbia (Grant Nos. 172013, 172035, and III45007).

References

1. Nakajima K, Ohta K, Katayanagi H, Mitsuke K. Photoexcitation and electron injection processes in azo dyes adsorbed on nanocrystalline TiO_2 films. Chemical Physics Letters 2011; 510 (4-6): 228-233. doi: 10.1016/j.cplett.2011.05.045
2. Han M, Zhang X, Zhang X, Liao C, Zhu B et al. Azo-coupled zinc phthalocyanines: towards broad absorption and application in dye-sensitized solar cells. Polyhedron 2015; 85: 864-873. doi: 10.1016/j.poly.2014.10.026
3. Mahmood A, Tahir MH, Irfan A, Al-Sehemi AG, Al-Assiri MS. Heterocyclic azo dyes for dye sensitized solar cells: a quantum chemical study. Computational and Theoretical Chemistry 2015; 1066: 94-99. doi: 10.1016/j.comptc.2015.05.020
4. Novir SB, Hashemianzadeh SM. Quantum chemical investigation of structural and electronic properties of trans- and cis-structures of some azo dyes for dye-sensitized solar cells. Computational and Theoretical Chemistry 2017; 1102: 87-97. doi: 10.1016/j.comptc.2017.01.009

5. Prajongtat P, Suramitr S, Nokbin S, Nakajima K, Mitsuke K et al. Density functional theory study of adsorption geometries and electronic structures of azo-dye-based molecules on anatase TiO_2 surface for dye-sensitized solar cell applications. Journal of Molecular Graphics and Modeling 2017; 76: 551-561. doi: 10.1016/j.jmgm.2017.06.002
6. Zhang L, Cole JM, Dai C. Variation in optoelectronic properties of azo dye-sensitized TiO_2 semiconductor interfaces with different adsorption anchors: carboxylate, sulfonate, hydroxyl and pyridyl groups. ACS Applied Materials & Interfaces 2014; 6 (10): 7535-7546. doi: 10.1021/am502186k
7. Zhang L, Cole J, Waddell P, Low K, Liu X. Relating electron donor and carboxylic acid anchoring substitution effects in azo dyes to dye-sensitized solar cell performance. ACS Sustainable Chemistry & Engineering 2013; 1 (11): 1440-1452. doi: 10.1021/sc400183t
8. Zhang L, Cole JM. TiO_2-assisted photoisomerization of azo dyes using self-assembled monolayers: case study on para-methyl red towards solar-cell applications. ACS Applied Materials & Interfaces 2014; 6 (5): 3742-3749. doi: 10.1021/am500308d
9. Zhang L, Cole JM, Liu X. Tuning solvatochromism of azo dyes with intramolecular hydrogen bonding in solution and on titanium dioxide nanoparticles. Journal of Physical Chemistry C 2013; 117 (49): 26316-26323. doi: 10.1021/jp4088783
10. Frisch MJ, Trucks GW, Schlegel HB, Scuseria GE, Robb MA et al. Gaussian 09, Revision D.01. Wallingford, CT, USA: Gaussian, Inc., 2009.
11. Becke AD. Density-functional thermochemistry. III. The role of exact exchange. Journal of Chemical Physics 1993; 98 (7): 5648-5652. doi: 10.1063/1.464913
12. Zhao Y, Truhlar DG. Density functionals with broad applicability in chemistry. Accounts of Chemical Research 2008; 41 (2): 157-167. doi: 10.1021/ar700111a
13. Barone V, Cossi M. Quantum calculation of molecular energies and energy gradients in solution by a conductor solvent model. Journal of Physical Chemistry A 1998; 102 (11): 1995-2001. doi: 10.1021/JP9716997
14. Wang Y, Zhou D, Li H, Li R, Zhong Y et al. Hydrogen-bonded supercoil self-assembly from achiral molecular components with light-driven supramolecular chirality. Journal of Materials Chemistry C 2014; 2 (31): 6402-6409. doi: 10.1039/c4tc00649f
15. Tuuttila T, Lipsonen J, Huuskonen J, Rissanen K. Chiral donor-π-acceptor azobenzene dyes. Dyes and Pigments 2009; 80 (1): 34-40. doi: 10.1016/j.dyepig.2008.04.007
16. Thayer FK. m-Nitrocinnamic acid. Organic Syntheses 1925; 5: 83. doi: 10.15227/orgsyn.005.0083
17. Faridoon, Edkins AL, Isaacs M, Mnkandhla D, Hoppe HC et al. Synthesis and evaluation of substituted 4-(N-benzylamino)cinnamate esters as potential anti-cancer agents and HIV-1 integrase inhibitors. Bioorganic & Medicinal Chemistry Letters 2016; 26 (15): 3810-3812. doi: 10.1016/j.bmcl.2016.05.023
18. Skinner WA, Schelstraete MGM, Baker BR. Potential anticancer agents. XLVIII. Analogs of chlorambucil. VI.2 Ring isomers. Journal of Organic Chemistry 1961; 26 (5): 1554-1557. doi: 10.1021/jo01064a060
19. Skinner WA, Schelstraete MGM, Baker BR. Potential anticancer agents. XLVIII. Analogs of chlorambucil. VI.2 Ring isomers. Journal of Organic Chemistry 1961; 26: 1554-1557. doi: 10.1021/jo01064a060
20. Fukuda H, Nishikawa K, Fukunaga Y, Okuda K, Kodama K et al. Synthesis of fluorescent molecular probes based on *cis*-cinnamic acid and molecular imaging of lettuce roots. Tetrahedron 2016; 72 (41): 6492-6498. doi: 10.1016/j.tet.2016.08.060
21. Skinner WA, Schelstraete MGM, Baker BR. Potential anticancer agents. XLVIII. Analogs of chlorambucil. VI. Ring isomers. The Journal of Organic Chemistry 1961; 26 (5): 1554-1556. doi: 10.1021/jo01064a060

22. Mirazizi F, Bahrami A, Haghbeen K, Zahiri HS, Bakavoli M et al. Rapid and direct spectrophotometric method for kinetics studies and routine assay of peroxidase based on aniline diazo substrates. Journal of Enzyme Inhibition and Medicinal Chemistry 2016; 31 (6): 1162-1169. doi: 10.3109/14756366.2015.1103234

23. Haba O, Itabashi H, Sato S, Machida K, Koda T et al. UV-induced stable planar alignment of nematic liquid crystals using a polypropyleneimine dendrimer having a mesogen consisting of cinnamate and azobenzene moieties. Molecular Crystals and Liquid Crystals 2015; 610 (1): 201-209. doi: 10.1080/15421406.2015.1026737

24. Folcia CL, Alonso I, Ortega J, Etxebarria J, Pintre I et al. Achiral bent-core liquid crystals with azo and azoxy linkages: structural and nonlinear optical properties and photoisomerization. Chemistry of Materials 2006; 18 (19): 4617-4626. doi: 10.1021/cm060256p

25. Ferreira GR, Garcia HC, Couri MRC, Dos Santos HF, de Oliveira LFC. On the azo/hydrazo equilibrium in Sudan I azo dye derivatives. Journal of Physical Chemistry A 2013; 117 (3): 642-649. doi: 10.1021/jp310229h

26. Esme A, Sagdinc SG, Yildiz SZ. Experimental and theoretical studies on Sudan Red G [1-?(2-?methoxyphenylazo)?-?2-?naphthol] and its Cu(II) coordination compound. Journal of Molecular Structure 2014; 1075: 264-278. doi: 10.1016/j.molstruc.2014.07.009

27. Ertan N, Gürkan P. Synthesis and properties of some azo pyridone dyes and their Cu (II) complexes. Dyes and Pigments 1997; 33 (2): 137-147. doi: 10.1016/S0143-7208(96)00044-7

28. Mijin D, Božić Nedeljković B, Božić B, Kovrlija I, Lađarević J et al. Synthesis, solvatochromism and biological activity of novel azo dyes bearing 2-pyridone and benzimidazole moieties. Turkish Journal of Chemistry 2018; 42 (3): 896-907. doi: 10.3906/kim-1711-97

29. Cinar M, Coruh A, Karaback M. A comparative study of selected disperse azo dye derivatives based on spectroscopic (FT-IR, NMR and UV-Vis) and nonlinear optical behaviors. Spectrochimica Acta Part A: Molecular and Biomolecular Spectroscopy 2014; 122: 682-689. doi: 10.1016/j.saa.2013.11.106

30. Dinçalp H, Toker F, Durucasu I, Avcibaşi N, Icli S. New thiopene-based azo ligands containing azo methane group in the main chain for determination of copper(II) ions. Dyes and Pigments 2007; 75 (1): 11-24. doi: 10.1016/j.dyepig.2006.05.015

31. Smitha P, Asha SK, Pillai CKS. Synthesis, characterization and hyperpolarizability measurements of main-chain azobenzene molecules. Journal of Polymer Science, Part A: Polymer Chemistry 2005; 43 (19): 4455-4468. doi: 10.1002/pola.20922

32. Gorelik MV, Rybinov VI, Gladysheva TK. Azo-quinone hydrazone tautomerism of 1-(arylazo)-2-naphthols and 2-(arylazo)-1-naphthols. Zhurnal Obshchei Khimii 1988; 58 (10): 2360-2370.

33. Fedorov LA, Sokolovskii SA. Carbon-13 NMR spectra and azo-quinone hydrazone tautomerism of azo derivates of 1- and 2-naphthol. Izvestiya Akademii Nauk SSSR, Seriya Khimicheskaya 1988; 10: 2271-2277.

34. Fabian WMF, Antonov L, Nedeltcheva D, Kamounah FS, Taylor PJ. Tautomerism in hydroxynaphthaldehyde anils and azo analogues: a combined experimental and computational study. Journal of Physical Chemistry A 2004; 108 (37): 7603-7612. doi: 10.1021/jp048035z

35. Antonov L, Fabian WMF, Taylor PJ. Tautomerism in some aromatic Schiff bases and related azo compounds: an LSER study. Journal of Physical Organic Chemistry 2005; 18 (12): 1169-1175. doi: 10.1002/poc.965

36. Christie RM. Colour Chemistry. Cambridge, UK: The Royal Society of Chemistry, 2015.

37. Chen XC, Tao T, Wang YG, Peng YX, Huang W et al. Azo-hydrazone tautomerism observed from UV-vis spectra by pH control and metal-ion complexation for two heterocyclic disperse yellow dyes. Dalton Transactions 2012; 41 (36): 11107-11115. doi: 10.1039/c2dt31102j

38. Mirković J, Rogan J, Poleti D, Vitnik V, Vitnik Ž et al. On the structures of 5-(4-, 3- and 2-methoxyphenylazo)-3-cyano-1-ethyl-6-hydroxy-4-methyl-2-pyridone: an experimental and theoretical study. Dyes and Pigments 2014; 104: 160-168. doi: 10.1016/j.dyepig.2014.01.007

39. Mijin D, Božić B, Lađarević J, Matović L, Uščumlić G et al. Solvatochromism and quantum mechanical investigation of disazo pyridone dye. Coloration Technology 2018; 134 (6): 478-490. doi: 10.1111/cote.12369

40. Zhang L, Cole JM. Can nitro groups really anchor onto TiO_2? Case study of dye-to- TiO_2 adsorption using azo dyes with NO_2 substituents. Physical Chemistry Chemical Physics 2016; 18 (28): 19062-19069. doi: 10.1039/c6cp02294d

41. Hug H, Bader M, Mair P, Glatzel T. Biophotovoltaics: natural pigments in dye-sensitized solar cells. Applied Energy 2014; 115: 216-225. doi: 10.1016/j.apenergy.2013.10.055

42. Chen Z, Li F, Huang C. Organic D-π-A dyes for dye-sensitized solar cell. Current Organic Chemistry 2007; 11 (14): 1241-1258. doi: 10.2174/138527207781696008

43. Khan MZH, Al-Mamuna MR, Halderb PK, Aziz MA. Performance improvement of modified dye-sensitized solar cells. Renewable and Sustainable Energy Reviews 2017; 71: 602-617. doi: 10.1016/j.rser.2016.12.087

44. Zhao GJ, Yu F, Zhang MX, Northrop BH, Yang H et al. Substituent effects on the intramolecular charge transfer and fluorescence of bimetallic platinum complexes. Journal of Physical Chemistry A 2011; 115 (24): 6390-6393. doi: 10.1021/jp202825q

45. Luque A, Hegedus S. Handbook of Photovoltaic Science and Engineering. Chichester, UK: John Wiley & Sons Ltd, 2003.